EXPLOITING POLE-LIKE OBJECTS FROM CADASTRES FOR SUB-METRE ACCURATE INTEGRATED GEOREFERENCING OF LOW-COST MOBILE MAPPING SYSTEMS

J. Meyer *, S. Nebiker, S. Schürmann, E. Ferrari, M. Ammann

Institute of Geomatics, FHNW University of Applied Sciences and Arts Northwestern Switzerland, Muttenz, Switzerland – (jonas.meyer, stephan.nebiker, elia.ferrari, manuela.ammann)@fhnw.ch, stefanschuermann@flashcable.ch

KEY WORDS: Georeferencing, Mobile Mapping, Urban, Localization, RGB-D, Depth Map, Point cloud, Pole-like objects.

ABSTRACT:

Accurately georeferenced data acquired using mobile mapping systems is of great importance for many geospatial applications. The accuracy of direct georeferencing – the standard procedure in the field of outdoor mobile mapping – strongly relies on GNSS reception and therefore varies greatly depending on the environment. By incorporating control point observations, integrated georeferencing enables homogenous accuracy and reliability over the whole mapping perimeter. Unfortunately, exact measurement and documentation of control points is needed, which often must be done manually. To automate this process, approaches from the field of autonomous vehicles use pole-like objects to support localization in complex urban environments, with the disadvantage of requiring a prior mapping campaign. However, various classes of pole-like objects have been recorded with accurate location and entered in public cadastres, so they could serve as 2D control points. In this paper, we present an approach for improving the trajectory accuracy in challenging urban environments by means of integrated georeferencing. It uses range image observations to pole-like objects from publicly available cadastres. Our approach achieves sub-metre accuracy, with a maximal cross-track difference of 98 cm, using real-world data acquired with our low-cost mobile mapping system. We further demonstrate that it significantly improves discontinuities and inaccuracy peaks in direct georeferencing and that the limiting factors are errors in the depth estimation of available range imaging sensors.

1. INTRODUCTION

A transformation of urban mobility from individual motorized transportation towards an increasing variety of multimodal mobility offerings is ongoing. This transformation is expected to result in a reduced need for on-street parking spaces. In addition, government agencies are interested in freeing street space, including areas currently occupied by on-street parking, to accommodate new bike lanes and other alternative modes of transportation. To provide automated, reliable base data in form of on-street parking statistics for government agency and policy makers Nebiker et al. (2021) developed a low-cost Mobile Mapping System (MMS) to cover entire cities with regular revisit capabilities. The system uses point clouds from range imaging sensors, edge computing and AI-based 3D object detection methods to detect vehicles directly on the MMS (Meyer et al., 2022). However, reliable on-street parking statistics require accurate georeferencing of the detected vehicles at the dm- to sub-metre-level (Nebiker et al., 2021). Direct georeferencing based on GNSS/INS sensor integration is the current technology of choice. However, in complex urban areas, even direct georeferencing using high-end system components can be affected by positioning errors of up to several metres due to multipath effects and GNSS signal obstruction (Eugster et al., 2012). Further investigations confirmed that the required sub-metre accuracy cannot be consistently ensured with low-cost system components (Nebiker et al., 2021). Therefore, other georeferencing methods are needed to ensure sub-metre accuracy in challenging urban environments.

On-street parking statistics are only one of many use cases supported by our low-cost MMS and its latest further development (Meyer et al., 2022). In particular, the modular and flexible architecture of the acquisition software allows additional mapping tasks to be carried out in parallel. To enable a variety of use cases, the new georeferencing method must meet several requirements: 1) it has to be real-time capable, 2) it has to provide absolute position and orientation parameters in a global reference frame, 3) it has to be computationally feasible to be executed in parallel to the mapping tasks, and 4) it has to provide area-wide sub-metre accuracy using low-cost sensors.

Integrated georeferencing (Eugster et al., 2012) is widely used to ensure homogenous accurate and reliable georeferencing over the entire mapping perimeter. By incorporating a number of ground control point (GCP) observations that have been accurately measured along the trajectory, integrated georeferencing refines the trajectory of direct georeferencing. It can achieve centimetre-level accuracy even in GNSS-denied areas such as tunnels or urban canyons depending on the accuracy of the used observation sensors and control points. However, integrated georeferencing places high demands on the exact measurement and documentation of control points, which often cannot be automated (Eugster et al., 2012; Cavegn et al., 2016).

With the aim to automate the process of control point determination and observation, various approaches from the field of autonomous navigation use pole-like objects to support localization in complex urban environments (Brenner, 2009; Spangenberg et al., 2016; Sefati et al., 2017; Schaefer et al., 2019). Due to their ubiquity, distinctiveness, and long-term stability, pole-like objects are well suited for localization or georeferencing approaches in urban scenarios. Although all approaches require no manual work, they have one major drawback. They all depend on a preliminary acquisition phase for mapping pole-like objects within the relevant perimeter.

* Corresponding author

Pole-like objects serve various purposes in cities, for example, as posts for street lighting, traffic signs and traffic lights, as a carrier of electricity for public transport, or simply in the form of trees. In Switzerland, especially in the city of Basel, many of these objects are recorded with accurate location and entered in a cadastre due to public interest. Thus, exactly determined and clearly identifiable pole-like objects are often available in public cadastres and could serve as 2D ground control points for robust and accurate georeferencing in urban areas.

In this contribution we present an approach for improving the trajectory accuracy by means of integrated georeferencing using range image observations to pole-like objects available in public cadastres. We evaluate this approach with real-world data from our low-cost mobile mapping system and present quantitative as well as qualitative results.

2. RELATED WORK

2.1 Georeferencing of mobile mapping data

Direct georeferencing (DG) generally refers to platform and sensor pose estimation using on-board sensors, which are independent from the mapping sensors. The combination of GNSS and INS raw data using a Kalman Filter is widely used for DG since the early days of MMS (Schwarz et al., 1993). Two predominant strategies, loosely coupled and tightly coupled sensor integration, have become established (Angrisano, 2010). While loosely coupled approaches process raw data from GNSS and INS independently and fuse them afterwards, tightly coupled approaches directly fuse the raw data from both sensors. Loosely coupled sensor integration has the advantage of shorter processing time, higher robustness, and independent navigation solutions. By contrast, tightly coupled sensor integration results in lower process noise and benefits even from GNSS satellite constellations with less than four satellites (Cramer, 2001). Thus, tightly coupled sensor integration is advantageous in areas with degraded GNSS reception (Angrisano, 2010). The accuracy of DG strongly depends on GNSS reception. In case of partial or total signal shading, i.e., in urban canyons, under dense tree canopies or in tunnels, the accuracy can decrease from the centimetre range to the decimetre or even metre range, also with high-end equipment (Cavegn et al., 2018). Therefore, DG works well in outdoor environments with good GNSS coverage. DG is also real-time capable and provides trajectories in a global reference frame.

To ensure homogeneous, accurate and reliable georeferencing across the entire mapping perimeter Eugster et al. (2012) propose **integrated georeferencing (IG)** method. This solution uses coordinate updates (CUPT) to support a loosely coupled sensor integration of GNSS and INS during GNSS outages (Eugster et al., 2012). A CUPT is obtained by applying the difference between the ground truth coordinates of the GCP and the GCP coordinates observed by the mapping sensors to the current pose. This results in a corrected trajectory, where the accuracy of the resulting trajectory depends on the accuracy of the GCP determination by the mapping sensors and the accuracy of the GCP ground truth coordinates. Eugster et al. (2012) demonstrated an improvement from decimetre- to centimetre-level in comparison with DG. IG provides a trajectory directly within a global reference frame, in real-time and with homogenous accuracy and reliability if enough GCPs are available. However, it places high demands on the exact initial measurement and documentation as well as on the subsequent observation of GCPs, which often cannot be automated (Eugster et al., 2012). Blaser (2022) adapted IG and used a tightly coupled sensor integration to calculate the trajectory of a portable MMS (Blaser et al., 2020).

Besides DG and IG also LiDAR- (Nüchter et al., 2015; Blaser et al., 2019; Karam et al., 2019; Blaser et al., 2020) and image-based (Cavegn et al., 2018; Blaser et al., 2020) georeferencing methods are used to determine MMS trajectories. However, these approaches provide trajectories in a local reference frame which must be transformed to the global reference frame via GCPs or additional GNSS observations if necessary. A comprehensive overview of the mentioned georeferencing strategies is given by Blaser (2022).

2.2 Pole-like objects for georeferencing tasks

Due to their ubiquity, distinctiveness and long-term stability, pole-like objects are well suited for localization or georeferencing approaches in urban scenarios. Moreover, thanks to their distinct geometric shape, they can easily be detected in data from cameras and LiDAR sensors even when they are partly obscured. Several approaches from the field of autonomous vehicles use pole-like objects to support localization in complex urban environments and to automate the processes of control point determination and control point observation. Pole-like objects are observed in LiDAR data (Brenner, 2009; Kümmerle et al., 2009; Weng et al., 2018; Schaefer et al., 2019; Chen et al., 2021), stereo images (Spangenberg et al., 2016) or both (Sefati et al., 2017). These observations are then fused with data from IMU, GNSS, vehicle odometry or other sensors using state estimation techniques such as Kalman filters or particle filters to obtain the vehicle poses. The resulting trajectory accuracies are stated to be all in the lower decimetre range. Although all approaches require no manual work, they have one major drawback. They all depend on a prior data acquisition phase in which pole-like objects within the relevant perimeter are captured and stored either directly as point cloud objects or as feature representations of any kind. This step is typically performed using an expensive high-end mobile mapping system. However, since the perimeter of interest is mapped in advance the proposed solutions have no necessity for poses within a global reference frame.

3. MATERIALS AND METHODS

3.1 Low-cost Mobile Mapping System (MMS)

In previous works we introduced a versatile low-cost MMS (Figure 1) and a corresponding postprocessing workflow for the creation of on street-parking statistics (Nebiker et al., 2021; Meyer et al., 2022).

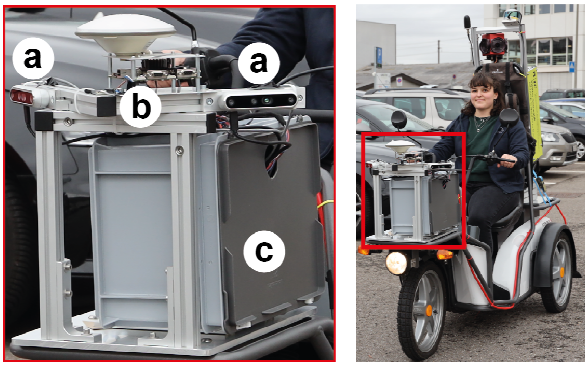

Figure 1. Mobile mapping system with low-cost sensor setup (Nebiker et al., 2021).

The MMS consists of an electric tricycle as mapping platform and a low-cost sensor setup on the front luggage carrier (Figure 1). The sensor setup integrates two Intel RealSense D455 RGB-D cameras (Intel Corporation, 2023) as mapping sensors (Figure 1, a), a consumer grade GNSS/IMU-based navigation unit SwiftNav Piksi Multi (Swift Navigation, 2019) (Figure 1, b) and a single-board computer (Figure 1, c). Nebiker et al. (2021) showed an average 2D localization accuracy in a challenging urban environment of 0.9 m, with peaks of over one metre in position and over 2.5 m in height. The peaks could be attributed to areas with poor GNSS signal coverage and clearly showed the limited performance of the used low-cost navigation unit.

3.1.1 Navigation unit

The GNSS- and IMU-based navigation unit SwiftNav Piksi Multi (Swift Navigation, 2019) consists of a multi-band and multi-constellation GNSS RTK receiver board and a geodetic GNSS antenna. The GNSS receiver board also includes the consumer-grade IMU Bosch BMI160 (Bosch Sensortec, 2020).

3.1.2 Depth camera

Besides the navigation unit, the accuracy of the mapping sensor Intel RealSense D455 (Intel Corporation, 2023) is crucial for this work. The camera acquires colour images as well as depth maps with a resolution of 1280 x 720 pixels and a frame rate of up to 30 Hz. The active stereo-based depth estimation range is specified from 0.4 to 10m, but may vary depending on lighting conditions, especially outdoors (Intel Corporation, 2023). The camera only provides an interface for external hardware-based triggering of the depth sensor, but not of the RGB image sensor. The resulting point clouds are very noisy compared to LiDAR data commonly used in mobile mapping applications.

Nebiker et al. (2021) evaluated the accuracy of the depth estimation for different Intel RealSense D455 cameras. They decoupled the depth error into bias and precision as proposed by Halmetschlager-Funek et al. (2019). The calculated bias and precision vary greatly between the cameras and in some cases exceed the specified value of 2% of the object distance by an order of magnitude. It has also been demonstrated that different cameras of the same type do not behave comparably. Therefore, an error model must be estimated or assumed for each camera independently. Based on the bias and precision parameters determined by Nebiker et al. (2021) and due to the lack of additional information about the long-term behaviour, we took the conservative assumption, that the depth estimation accuracy is around 8% of the estimated depth value.

3.2 Study area and data

The study area represents a typical European city in terms of building heights, street widths and vegetation. In the study area, a 7.95 km trajectory (Figure 2, black line) was traversed with our MMS in the summer of 2021 three times on the same day – at noon, in the afternoon, and in the. At the beginning and the end of each campaign the system was initialized in a location with good GNSS coverage (Figure 2, start/stop). During the campaigns, RGB-D images were acquired with 5 frames per seconds (fps), resulting in an average distance between two consecutive images of around 1 metre. Due to a problem with the bandwidth of the USB interface of the on-board computer, only the data from the camera pointing to the right has been collected. For this paper, only the data from the noon campaign are considered, which comprises at total of 9187 RGB-D images.

3.3 Reference data

3.3.1 Reference trajectory

To obtain an accurate reference trajectory (Figure 2, black line), we performed image-based georeferencing (Cavegn et al., 2016; Blaser et al., 2020) in Agisoft Metashape (Agisoft, 2023) for all colour images using pose priors from DG.

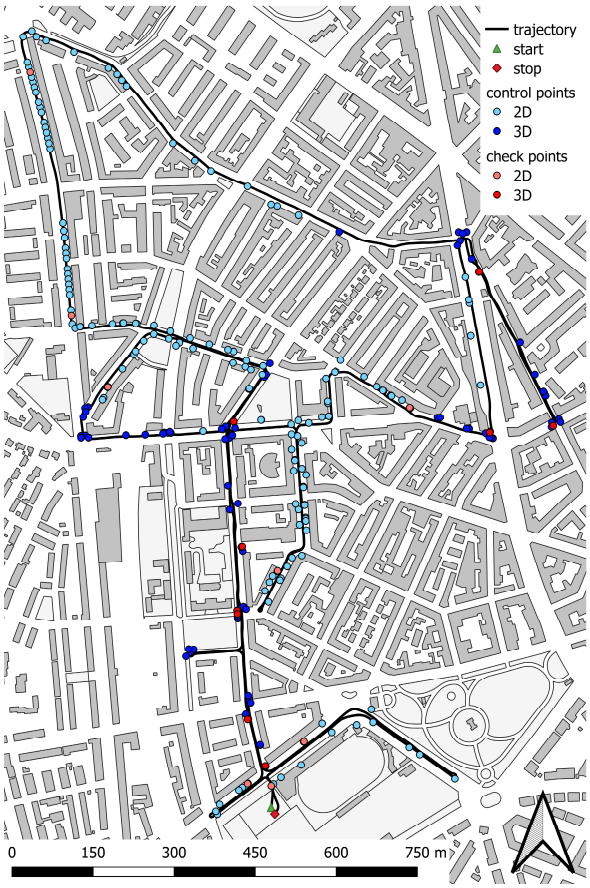

Figure 2. Reference trajectory (black) obtained from image-based georeferencing and the used control points (3D blue; 2D light blue) and check points (3D red; 2D light red) (data source: Geodaten Kanton Basel-Stadt)

	RMSE E [m]	RMSE N [m]	RMSE H [m]
Control points	0.038	0.036	0.032
Check points	0.043	0.032	0.037

Table 1. RMSE of image-based georeferencing of the reference trajectory for each coordinate dimension (E = easting, N = northing, H = height)

For image-based georeferencing a total of 237 control points were incorporated, of which 155 were determined in 2D and 82 in 3D. Additionally, 17 check points were used to verify the georeferencing quality independently. 8 of the check points were determined in 2D and 9 in 3D. Control and check points were measured manually in at least eight images. We achieved RMSE values of the image-based georeferencing in each coordinate dimension of 3-4 cm (Table 1).

The control and check points used are natural, clearly visible, and recognizable features such as base points of traffic signs, curb corner points as well as window or balcony corners. The coordinates of the 3D control and check points were measured

using a Leica GS18I GNSS system (Leica Geosystems AG, 2022) in RTK-mode. The accuracy of these points is around 2-3 cm. The coordinates of the 2D control and check points were obtained from the official cadastre of the city of Basel. Since this cadastre was proven to be very accurate, the accuracy of these points is subsequently assumed to be better than 5 cm.

3.3.2 Pole-like objects from cadastre

In the city of Basel, pole-like objects are included in the tree and electricity cadastres. The tree cadastre contains all trees along roads or in parks with a location coordinate for the centre of the trunk at ground level and various attributes such as age, year of planting, species, etc. However, no information about the trunk diameter is included (Kanton Basel-Stadt, 2023).

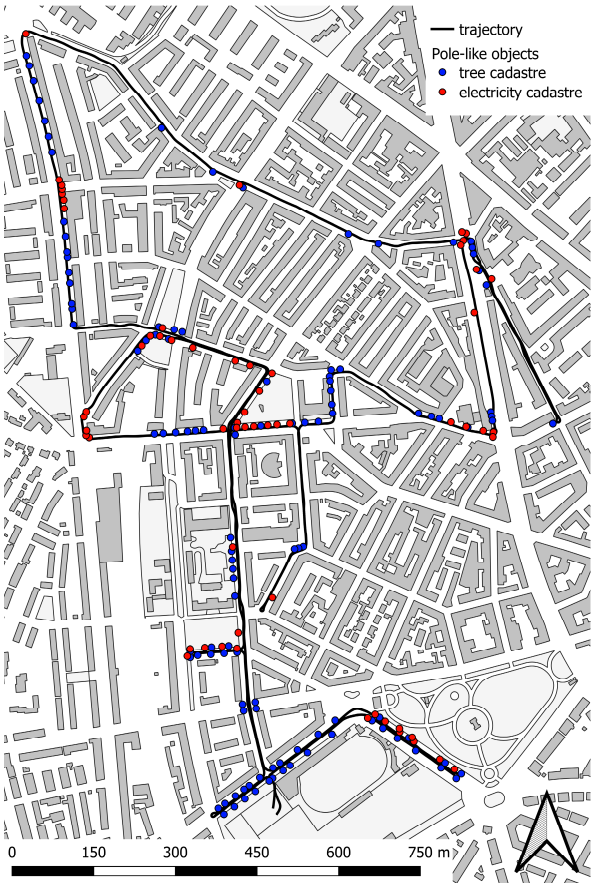

Figure 3. Pole-like objects used for trajectory processing divided into two classes: trees (blue points) and electricity poles (red points) (data source: Geodaten Kanton Basel-Stadt)

The electricity cadastre includes – apart from the electricity infrastructure in the underground – all electricity-related objects above ground, such as distribution boxes, traffic lights, traffic safety installations and electricity supply for public transportation. Several of these objects are of pole-like shape. Each pole-like object in the electricity cadastre has an accurate 2D coordinate representing the centre of the pole as well as information about its diameter (Kanton Basel-Stadt, 2023).

Both datasets were obtained from the land registry and survey office of the canton Basel-Stadt. By using a buffer of 12 metres around the reference trajectory all potentially usable pole-like objects along the trajectory were determined, resulting in a total of 668 objects (Table 2). Since we only observed the right side in direction of motion, many of these objects were not captured. We then manually measured all visible poles from the electricity cadastre and various trees in well-suited locations in the depth maps (Table 2, Figure 3). In the remainder of this paper, we refer to trees and poles instead 'pole-like objects from the tree and electricity cadastre' respectively.

	poles	tree
along trajectory	157	511
measured in depth maps	66	118

Table 2. Number of pole-like objects in the vicinity of the trajectory and number of objects measured in the depth maps.

As can be seen in Figure 3, trees are present in many places along the trajectory. In contrast, poles occur only sporadically and mostly in groups. Groups of poles typically represent intersections of main roads where traffic lights as well as other safety installations are present. Furthermore, there are poles where there is a lack of buildings and infrastructure for attaching the power supply for public transportation.

3.4 Georeferencing methods

3.4.1 Direct georeferencing

For DG a combined tightly coupled forward and backward processed GNSS and IMU sensor data fusion and trajectory processing is performed in Waypoint Inertial Explorer (NovAtel, 2020). By interpolating the precise trigger timestamps of the camera triggering and by considering lever arm and misalignment between the navigation centre and the camera we obtain georeferenced poses for each depth map.

3.4.2 Integrated georeferencing using pole-like objects

For IG using pole-like objects, we apply the workflow described in Blaser (2022), which relies on an undocumented legacy feature of Inertial Explorer (NovAtel, 2020). First, DG is performed as described above. Then the 3D coordinates of the observed GCPs are calculated via the known interior camera geometry and the depth values and are subsequently transformed into the superordinate reference frame via the camera pose. The camera pose from DG is then corrected by the 2D coordinate difference between the ground truth and the observed coordinates of the GCP. A Python-based tool by Blaser (2022) creates the CUPTs based on the corrected camera poses. Additionally, each coordinate component can be weighted individually. Thus, the observation error is specified as weight for the 2D position. The observation error is calculated using the error model of the depth camera and an additional error term for the pole-like object. The errors are added quadratically (1).

$$err_{x,y} = \sqrt{err_{cam}{}^2 + err_{pole}{}^2} \quad , \tag{1}$$

The created coordinate updates are then integrated into Inertial Explorer and a combined tightly coupled forward and backward processed GNSS and IMU sensor data fusion and trajectory processing is performed. The resulting poses for the depth sensor are obtained by applying lever arm and misalignment.

3.5 Trajectory comparison

Due to the lack of an interface for external hardware-based triggering of the RGB sensor, colour and depth images are not exactly synchronized. Thus, an unknown time delay between

colour images and depth maps is present, leading to along-track differences of up to around 50 cm. For this reason, common evaluation metrics such as absolute trajectory error (ATE) and relative pose error (RPE) (Sturm et al., 2012) are not applicable. Moreover, a comparison of the rotational part of the poses is also not possible. Therefore, the quality of the georeferencing methods is assessed based on the cross-track differences between the resulting trajectory and the reference trajectory.

4. EXPERIMENTS AND RESULTS

4.1 Accuracy of cadastral pole-like objects

To evaluate the accuracy of the coordinates of the pole-like objects within the electricity cadastre, we measured 20 different pole objects with a Leica GS18I GNSS system (Leica Geosystems AG, 2022) in RTK mode. The comparison of the coordinates showed an average 2D difference of less than 10 cm. The accuracy of tree centre coordinates within the tree cadastre is considered as accurate as pole-like objects from the electricity cadastre. However, since there is no information about the trunk diameter of the tree, which also varies greatly depending on the height above the ground, and since trees usually do not grow exactly vertically, a conservative accuracy of the tree centre coordinates of 0.5 meter is assumed for this work.

4.2 Georeferencing methods

4.2.1 Direct georeferencing

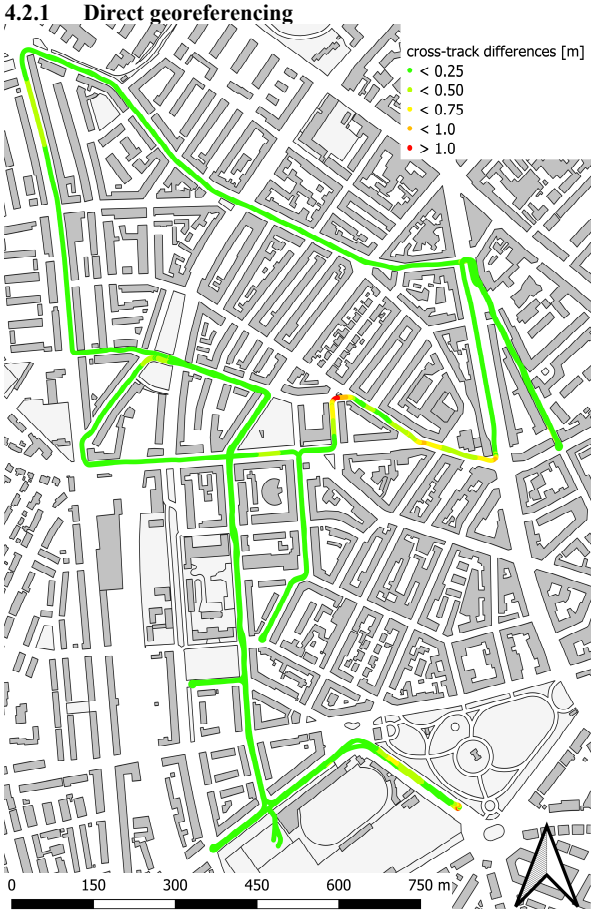

Figure 4. Cross-track differences of DG. Cross-track differences are colourized by their length (data source: Geodaten Kanton Basel-Stadt)

DG was processed as described before. Figure 4 shows the cross-track differences between the directly georeferenced trajectory and the reference trajectory colourized by their length. 99% of the trajectory has a cross-track difference of less than 65 cm to the reference trajectory, 95% even less than 37 cm (Figure 4 green and yellow parts of trajectory, Table 3). However, there are some areas, where the cross-track differences reach or even exceed one metre with a maximum of 1.17 m (Figure 4 orange and red parts of trajectory, Table 3).

median [m]	quantile 95% [m]	quantile 99% [m]	max value [m]
0.036	0.370	0.648	1.169

Table 3. Summary of cross-track differences of directly georeferenced trajectory vs. reference trajectory.

4.2.2 Integrated georeferencing using pole-like objects

Since CUPTs from trees are assumed to be less accurate than CUPTs from poles, we processed two different trajectories with our proposed IG approach. In the first processing, we incorporated coordinate updates from trees and poles, while in the second, we included poles only. Both trajectories were processed as described in section 3.4.2 using 10 cm and 50 cm as position error values for poles and trees respectively.

Integrated georeferencing using poles and trees

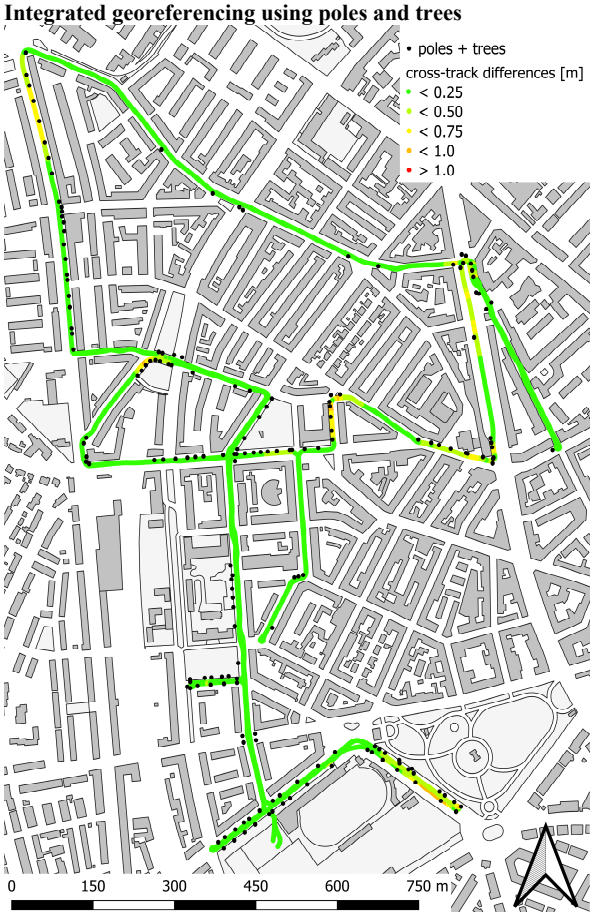

Figure 5. Cross-track differences of IG using poles and trees (black dots). Cross-track differences are colourized by their length (data source: Geodaten Kanton Basel-Stadt)

IG using poles and trees was processed leveraging CUPTs for 1264 camera poses created from measurements of 66 poles and

118 trees (Figure 5, black dots). The cross-track differences of the resulting trajectory are all smaller than 1 metre with a maximum value of 98 cm (Figure 5, Table 4). The 95% and 99% quantiles are 50 and 74 cm respectively (Table 4).

median [m]	quantile 95% [m]	quantile 99% [m]	max value [m]
0.036	0.496	0.739	0.981

Table 4. Summary of cross-track differences of IG using all poles and trees vs. reference trajectory.

Integrated georeferencing using poles only

For IG using poles only, a total of 484 CUPTs created from measurements of 66 poles were incorporated (Figure 6, black dots). 99% of the trajectory has a cross-track difference of less than 60 cm to the reference trajectory, 95% even less than 40 cm (Table 5). The maximum cross-track difference is 1.14 m (Figure 6 red part of trajectory, Table 5).

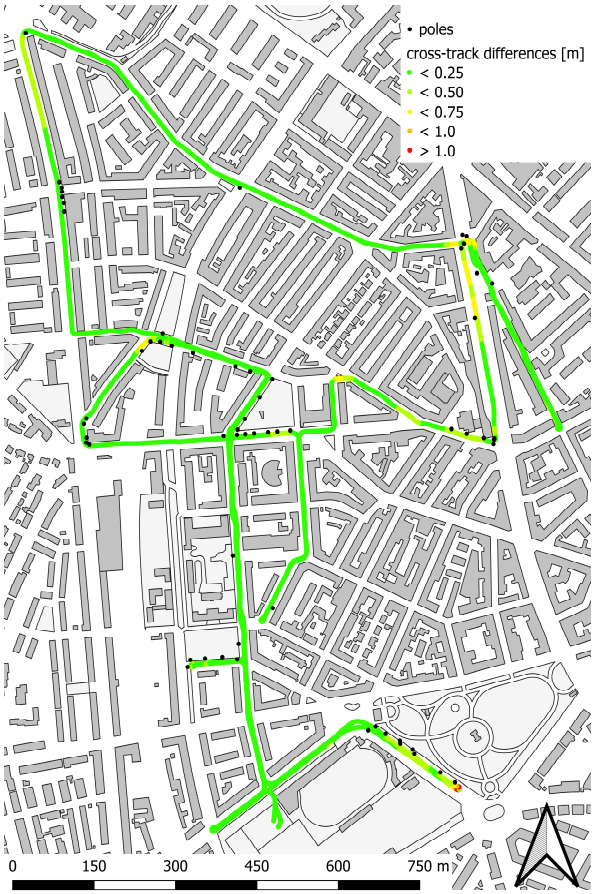

Figure 6. Cross-track differences of IG using poles only (black dots). Cross-track differences are colourized by their length (data source: Geodaten Kanton Basel-Stadt)

median [m]	quantile 95% [m]	quantile 99% [m]	max value [m]
0.037	0.402	0.599	1.137

Table 5. Summary of cross-track differences of IG using poles only vs. reference trajectory.

4.2.3 Comparison of georeferencing in selected areas

To assess the potential and challenges of the proposed IG approach, a closer look at selected areas of the trajectory is necessary. The accuracy of DG is usually compromised by strong GNSS signal obstruction. In combination with long standstills or very slow motion the resulting trajectory has a poor accuracy, possibly with discontinuities.

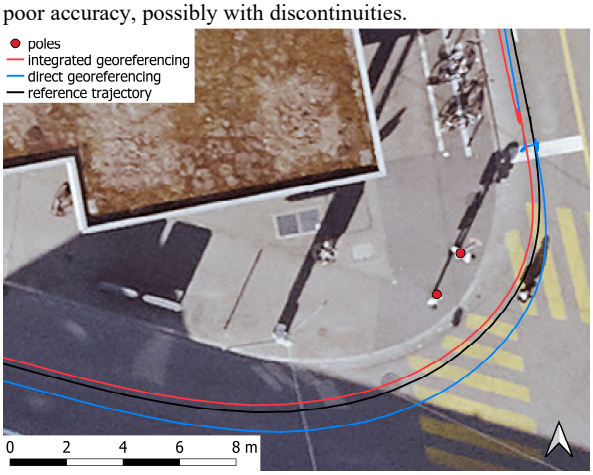

Figure 7. Improvement of IG (red line) using poles (red dots) over DG (blue line) during a phase with slow motion and a standstill combined with strong GNSS signal obstructions in front of a traffic light (data source: Geodaten Kanton Basel-Stadt)

Figure 7 shows a crossroad where the trajectory from DG (Figure 7, blue line) has a strong discontinuity because of a phase with slow motion and a standstill of about 38 seconds in front of a traffic light. Additionally, several high buildings are situated around the crossroad, causing significant GNSS signal obstructions. Our IG approach reduces the drift and produces a significantly more continuous trajectory (Figure 7, red line). However, small discontinuities are still apparent. The higher accuracy of IG is also evident from the key statistical indicators (Table 6) calculated for the cross-track differences in Figure 7. The maximum, quantile 95% and the 99% quantile values of IG are about 40% smaller than those of DG (Table 6).

georeferencing	DG	IG
median [m]	0.386	0.348
quantile 95% [m]	0.713	0.433
quantile 99% [m]	0.787	0.450
max value [m]	0.800	0.464

Table 6. Summary of cross-track differences for direct and IG for the subset of the trajectory depicted in Figure 7.

There are other areas with GNSS signal obstructions like the one shown in Figure 8. There the trajectory leads through a narrow street lined with trees forming a dense canopy. At the southern end of the street (Figure 8, bottom) there is a large square with no signal obstruction. At the northern end there is a small square with trees and a building to the south, also causing GNSS signal obstructions. As expected, also in this case DG was degraded under these conditions, exhibiting peaks with high inaccuracies (Figure 8, a). IG using poles and trees as well as poles only reduced the peak of inaccuracy significantly (Figure 8 b & c, Table 7). However, IG using poles and trees (Figure 8, b) deviates significantly from the reference trajectory in the region where tree based CUPTs were incorporated.

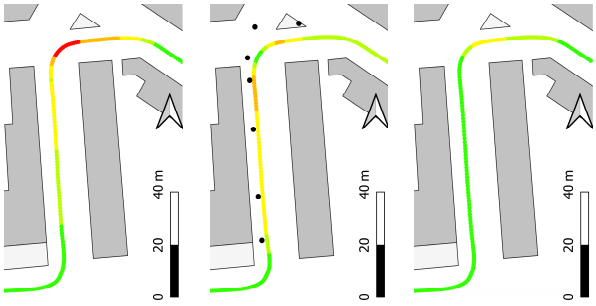

a) **b)** **c)**

Figure 8. Comparison of trajectories from **a)** DG, **b)** IG using poles + trees and **c)** IG using poles only in an area with GNSS signal obstructions. Cross-track differences are colourized by their length, pole-like objects used are displayed as black dots. (data source: Geodaten Kanton Basel-Stadt)

georeferencing	DG	IG (poles + trees)	IG (poles)
median [m]	0.512	0.535	0.081
quantile 95% [m]	1.110	0.789	0.572
quantile 99% [m]	1.163	0.800	0.602
max value [m]	1.169	0.808	0.606

Table 7. Summary of cross-track differences for DG, IG using poles and trees and IG using poles only for the subset of the trajectory depicted in Figure 8.

5. DISCUSSION

IG using pole-like objects from cadastre data has the potential to provide fully automated and accurate georeferencing of mobile mapping data. By using pole-like objects inventoried in publicly available cadastres, the need for preliminary mapping of such objects across entire cities is eliminated. In Swiss public cadastres, objects are typically recorded in two dimensions without height information. Consequently, the accuracy of the height component achieved using cadastral pole-like objects for IG is similar to the height accuracy of DG. Pole-like objects are assumed to be stable over a long period of time. However, the timeliness of the reference data remains a critical factor.

By using poles and trees as support information in IG, we achieved the targeted accuracy of better than one metre for the entire trajectory (Table 4, Figure 5). However, it can be assumed that long-track differences will also occur, so that the total 2D position error might slightly exceed the 1 m goal in some cases.

The investigations have shown that discontinuities and peaks of inaccuracies can be significantly improved by IG using pole-like objects (Figure 7 & 8, Table 6 & 7). The investigations further demonstrated that the definition and determination accuracy of pole-like objects has a direct influence on the accuracy of the resulting trajectory. This is nicely depicted in Figure 8, where the observations of the trees used were likely inaccurate and led to a trajectory with a lower accuracy compared to DG. However, it is unclear yet whether the inaccurate observations arise from inaccurate reference data, including unknown tree diameters, or from incorrect depth values derived from the camera. In general, the results of IG using 'poles only' show that an increase in accuracy can be expected with more accurate and better defined GCPs (Figure 6, Table5). Comparing the 95% and 99% quantile values of the IG using poles only (Table 5) and IG using poles and trees (Table 4) an improvement of about 20% is observed.

The accuracy of pole-like objects in the order of 10 cm can be considered as excellent, which most likely will not be available in other cities. Consequently, it can be inferred that the mapping sensor is the primary factor affecting the accuracy of our IG approach. The used Intel RealSense D455 RGB-D camera has a specified bias and precision of 2% of the object distance, which would be acceptable. In reality, however, the investigated cameras of this type show significantly larger errors in depth estimation and are not comparable with each other. This makes the determination of a suitable error model difficult.

The results obtained in this paper are to be considered as a base-line, since we performed a combined forward and backward processing. In real-time applications, only the part of the trajectory already covered is available, which leads to a less accurate directly georeferenced pose. Hence, we expect the proposed IG approach to produce an even greater improvement over DG in real-time scenarios.

6. CONCLUSION AND OUTLOOK

In this paper, we presented an approach for improving the trajectory accuracy of an MMS in demanding urban areas by means of IG using range image observations to pole-like objects. We showed that pole-like objects inventoried in publicly available cadastres are suitable 2D GCPs for supporting IG and have the potential to fully automate the georeferencing process – even eliminating the need for a preliminary mapping phase of areas of interest. The proposed IG using pole-like objects from cadastres can reach the targeted sub-metre accuracy over the entire trajectory with the employed low-cost sensors. We also demonstrated that discontinuities and peaks of inaccuracies from DG can be significantly improved by our approach. However, the large depth estimation error of our RGB-D mapping sensor led to new areas of inaccuracies.

In future work we intend to examine our approach for real-time applications and will therefore investigate the accuracy of forward processing only. In addition, extensive accuracy investigations of our mapping sensors, including long-term stability as well as behaviour during long campaigns, would lead to better error models for the creation of CUPTs. Another component towards a fully automated georeferencing approach is the robust automatic detection of pole-like objects in the range imaging data provided by our MMS.

REFERENCES

Agisoft, (2023). Metashape Software, Version 1.8.5. https://www.agisoft.com/ (17 April 2023).

Angrisano, A., 2010. GNSS/INS Integration Methods. PhD Thesis, Dipartimento di Scienze Applicate, Universita Degli Studi Di Napoli "Parethenope".

Blaser, S., Meyer, J., Nebiker, S., Fricker, L., Weber, D., 2020. Centimetre-accuracy in forests and urban canyons – combining a high-performance image-based mobile mapping backpack with new georeferencing methods. *ISPRS Ann. Photogramm. Remote Sens. Spatial Inf. Sci.*, V-1–2020, 333–341. doi.org/10.5194/isprs-annals-V-1-2020-333-2020.

Blaser, S., Nebiker, S., Wisler, D., 2019. Portable image-based high performance mobile mapping system in underground environments – system configuration and performance evaluation. *ISPRS Annals of the Photogrammetry, Remote Sensing and Spatial Information Sciences*, IV-2/W5, 255–262. doi.org/10.5194/isprs-annals-IV-2-W5-255-2019.

Blaser, S., 2022. Multi-environment Georeferencing of RGB-D Panoramic Images from Portable Mobile Mapping – a Perspective for Infrastructure Management. PhD Thesis, Karlsruhe Institute of Technology (KIT), Karlsruhe, Germany. doi.org/ 10.5445/IR/1000151555.

Bosch Sensortec, 2020. BMI160. https://www.bosch-sensortec.com/media/boschsensortec/downloads/datasheets/bst-bmi160-ds000.pdf (17 April 2023).

Brenner, C., 2009. Global Localization of Vehicles Using Local Pole Patterns. In J. Denzler, G. Notni, H. Süße (Eds.), *Pattern Recognition*,61–70. Berlin, Heidelberg: Springer Berlin Heidelberg. doi.org/10.1007/978-3-642-03798-6_7.

Cavegn, S., Blaser, S., Nebiker, S., Haala, N., 2018. Robust and accurate image-based georeferencing exploiting relative orientation constraints. *ISPRS Annals of the Photogrammetry, Remote Sensing and Spatial Information Sciences*, IV–2, 57–64. doi.org/10.5194/isprs-annals-IV-2-57-2018.

Cavegn, S., Nebiker, S., Haala, N., 2016. A Systematic Comparison of Direct and Image-based Georeferencing in Challenging Urban Areas. *ISPRS - International Archives of the Photogrammetry, Remote Sensing and Spatial Information Sciences, XLI-B1*, 529–536. doi.org/10.5194/isprsarchives-XLI-B1-529-2016.

Chen, G., Lu, F., Li, Z., Liu, Y., Dong, J., Zhao, J., Yu, J, Knoll, A., 2021. Pole-Curb Fusion Based Robust and Efficient Autonomous Vehicle Localization System with Branch-and-Bound Global Optimization and Local Grid Map Method. *IEEE Transactions on Vehicular Technology*, 70(11), 11283–11294. doi.org/10.1109/TVT.2021.3114825.

Cramer, M., 2001. Genauigkeitsuntersuchungen zur GPS/INS-Integration in der Aerophotogrammetrie. PhD Thesis, Fakultät für Bauingenieur- und Vermessungswesen der Universität Stuttgart, Stuttgart, Germany.

Eugster, H., Huber, F., Nebiker, S., Gisi, A., 2012. Integrated georeferencing of stereo image sequences captured with a stereovision mobile mapping system – approaches and practical results. *Int. Arch. Photogramm. Remote Sens. Spatial Inf. Sci*., XXXIX-B1, 309–314. doi.org/10.5194/isprsarchives-XXXIX-B1-309-2012.

Halmetschlager-Funek, G., Suchi, M., Kampel, M., Vincze, M., 2019. An Empirical Evaluation of Ten Depth Cameras: Bias, Precision, Lateral Noise, Different Lighting Conditions and Materials, and Multiple Sensor Setups in Indoor Environments. *IEEE Robotics & Automation Magazine*, 26(1), 67–77. doi.org/10.1109/MRA.2018.2852795.

Intel Corporation, 2023. Intel®RealSense - Product Family D400 Series: Datasheet. https://dev.intelrealsense.com/docs/-intel-realsense-d400-series-product-family-datasheet (17 April 2023).

Kanton Basel-Stadt, 2023. Geodaten-Katalog. https://www.geo.bs.ch/geodaten/geodaten-katalog.html (17 April 2023).

Karam, S., Vosselman, G., Peter, M., Hosseinyalamdary, S., Lehtola, V., 2019. Design, Calibration, and Evaluation of a Backpack Indoor Mobile Mapping System. *Remote Sensing*, 11(8), 905. doi.org/10.3390/rs11080905.

Kümmerle, R., Steder, B., Dornhege, C., Ruhnke, M., Grisetti, G., Stachniss, C., Kleiner, A., 2009. On measuring the accuracy of SLAM algorithms. *Autonomous Robots*, 27(4), 387–407. doi.org/10.1007/s10514-009-9155-6.

Leica Geosystems AG, 2022. *Leica GS18 I Data sheet*.

Meyer, J., Blaser, S., Nebiker, S., 2022. AI-based 3d detection of parked vehicles on a mobile mapping platform using edge computing. *Int. Arch. Photogramm. Remote Sens. Spatial Inf. Sci*., XLIII-B1-2022, 437–445. doi.org/10.5194/isprs-archives-XLIII-B1-2022-437-2022.

Nebiker, S., Meyer, J., Blaser, S., Ammann, M., Rhyner, S., 2021. Outdoor Mobile Mapping and AI-Based 3D Object Detection with Low-Cost RGB-D Cameras: The Use Case of On-Street Parking Statistics. *Remote Sensing*, 13(16), 3099. doi.org/10.3390/rs13163099.

NovAtel, 2020. Inertial Explorer 8.9 User Manual. https://novatel.com/support/waypoint-software/inertial-explorer (14 April 2023).

Nüchter, A., Borrmann, D., Koch, P., Kühn, M., May, S., 2015. A man-portable, imu-free mobile mapping system. *ISPRS ISPRS Ann. Photogramm. Remote Sens. Spatial Inf. Sci.*, II-3/W5, 17–23. doi.org/10.5194/isprsannals-II-3-W5-17-2015.

Schaefer, A., Buscher, D., Vertens, J., Luft, L., Burgard, W., 2019. Long-Term Urban Vehicle Localization Using Pole Landmarks Extracted from 3-D Lidar Scans. *2019 European Conference on Mobile Robots (ECMR)*, 1–7. Prague, Czech Republic: IEEE. doi.org/10.1109/ECMR.2019.8870928.

Schwarz, K. P., Martell, H. E., El-Sheimy, N., Li, R., Chapman, M. A., Cosandier, D., 1993. VIASAT - A Mobile Highway Survey System of High Accuracy. *Proceedings of the Vehicle Navigation and Information Systems Conference*, 476–481. Ottawa: IEEE.

Sefati, M., Daum, M., Sondermann, B., Kreiskother, K. D., Kampker, A., 2017. Improving vehicle localization using semantic and pole-like landmarks. *2017 IEEE Intelligent Vehicles Symposium (IV)*, 13–19. Los Angeles, CA, USA: IEEE. doi.org/10.1109/IVS.2017.7995692.

Spangenberg, R., Goehring, D., Rojas, R., 2016. Pole-based localization for autonomous vehicles in urban scenarios. *IEEE International Conference on Intelligent Robots and Systems (IROS)*, 2161–2166. Daejeon, South Korea: IEEE. doi.org/10.1109/IROS.2016.7759339.

Sturm, J., Engelhard, N., Endres, F., Burgard, W., Cremers, D., 2012. A benchmark for the evaluation of RGB-D SLAM systems. *IEEE International Conference on Intelligent Robots and Systems*, 573–580. IEEE. doi.org/10.1109/IROS.2012.6385773.

Swift Navigation, Inc. 2019. PiksiMulti GNSS Module Hardware Specification. https://www.swiftnav.com/latest/piksi-multi-hw-specification (13 April 2023).

Weng, L., Yang, M., Guo, L., Wang, B., Wang, C., 2018. Pole-Based Real-Time Localization for Autonomous Driving in Congested Urban Scenarios. *IEEE International Conference on Real-Time Computing and Robotics (RCAR)*, 96–101. Kandima, Maldives: IEEE. doi.org/10.1109/RCAR.2018.8621688.